Journal of Power Sources 271 (2014) 108–113

Contents lists available at ScienceDirect

Journal of Power Sources

journal homepage: www.elsevier.com/locate/jpowsour

Counter electrodes from binary ruthenium selenide alloys for dye-sensitized solar cells

Pinjiang Li [a], Hongyuan Cai [b, *], Qunwei Tang [b, *], Benlin He [b], Lin Lin [c]

[a] Institute of Surface Micro and Nano Materials, Xuchang University, Xuchang 461000, Henan Province, PR China
[b] Institute of Materials Science and Engineering, Ocean University of China, Qingdao 266100, Shandong Province, PR China
[c] National Engineering Research Center for Nanotechnology, Shanghai 200241, PR China

HIGHLIGHTS

- Binary Ru–Se alloy CEs are prepared by a mild hydrothermal reduction method.
- The counter electrode from RuSe alloy CE has superior electrocatalytic activity.
- A power conversion efficiency of 7.15% is recorded from RuSe alloy CE based DSSC.
- The new concept is instructive in designing efficient and cost-effective DSSCs.

GRAPHICAL ABSTRACT

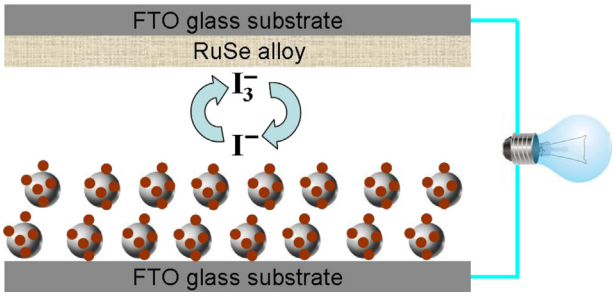

ARTICLE INFO

Article history:
Received 28 April 2014
Received in revised form
23 July 2014
Accepted 28 July 2014
Available online 2 August 2014

Keywords:
Dye-sensitized solar cell
Ruthenium selenide
Binary alloy
Counter electrode
Nanostructure

ABSTRACT

Dye-sensitized solar cell (DSSC) is a promising solution to global energy and environmental problems because of its merits on clean, cost-effectiveness, relatively high efficiency, and easy fabrication. However, the reduction of fabrication cost without sacrifice of power conversion efficiencies of the DSSCs is a golden rule for their commercialization. Here we design a new binary ruthenium selenide (Ru–Se) alloy counter electrodes (CEs) by a low-temperature hydrothermal reduction method. The electrochemical behaviors are evaluated by cyclic voltammogram, electrochemical impedance, and Tafel measurements, giving an optimized Ru/Se molar ratio of 1:1. The DSSC device with RuSe alloy CE achieves a power conversion efficiency of 7.15%, which is higher than 5.79% from Pt-only CE based DSSC. The new concept, easy process along with promising results provide a new approach for reducing cost but enhancing photovoltaic performances of DSSCs.

1. Introduction

Dye-sensitized solar cells (DSSCs) demonstrate advantages over other solar cells due to simple fabrication procedures, environmental friendliness, and relatively high power conversion efficiency [1–3]. As a key component, the counter electrode (CE) plays a role of collecting electrons from external circuit and catalyzing the reduction reaction of redox electrolyte ($I_3^- \rightarrow I^-$) [4–6]. Fluorine-doped tin oxide (FTO) conductive glass supported Pt is an effective CE for DSSC devices, however, the high cost from limited resource has been one of the main restrictions for DSSC commercialization [7]. By addressing this issue, it is a prerequisite to develop alternative CEs with low cost as well as high conduction, electrocatalysis, and readily availability.

* Corresponding authors. Tel./fax: +86 532 66781690.
E-mail addresses: chy_ouc08@sina.com (H. Cai), tangqunwei@ouc.edu.cn (Q. Tang).

http://dx.doi.org/10.1016/j.jpowsour.2014.07.175
0378-7753/

Moreover, the DSSCs assembled from such alternative CEs should have high power conversion efficiencies in comparison with that from Pt CE.

To date, conducting polymers (such as polyaniline and polypyrrole) [8–10], carbon materials (such as graphene and carbon nanotube) [11–13], or their composites have been widely employed as CE candidates due to their good electrocatalytic activity, low cost, simple synthesis, versatile processability, high electrical conductivity, and good environmental stability. Because of the relatively low electron-conduction of conducting polymers and low electrocatalysis of carbon materials, their composites are believed to combine the merits of single components. However, previous researches are focusing on chemical, physical or electrochemical combination [14,15]. The disadvantage of the proposed approaches is relatively high interfacial resistance between conducting polymers and carbon materials, which gives a low charge-transfer kinetics. In our previous reports [16–19], we proposed a reflux synthesis of conducting polymer/carbon material complexes, in which conducting polymers were bonded onto carbon materials via covalent bonding between N atoms (electron donor) and C atoms (electron acceptor). The power conversion efficiencies of the resultant DSSCs were also significantly enhanced in comparison with those using traditional composite CEs. More recently, Ma and coworkers have reported the employment of carbides, nitrides, and oxides as effective CE materials in catalyzing I_3^-/I^-, T_2/T^-, Co^{3+}/Co^{2+} redox couples [20]. Recently, binary alloys from Au–Ag have been employed as counter electrode material in DSSC, demonstrating a conversion efficiency of 7.85% [21]. More recently, we have reported the synthesis of low-Pt alloy CEs by an electrochemical deposition route for efficient DSSC application, giving an impressive efficiency of 10.23% from $CoPt_{0.02}$ alloy CE [22,23]. Also, a series of Pt–Ru alloys were deposited onto conductive glass substrate by a hydrothermal reduction method, showing an efficiency of 6.80% from $PtRu_3$ alloy CE based DSSC [24]. Although the research on binary alloy CEs is in a preliminary state, the impressive photovoltaic performances have demonstrated them to be good alternatives for DSSC application.

In the search for a new class of efficient and cost-effective CEs, we report here the employment of binary ruthenium selenide (Ru–Se) alloys as a way to replace Pt without sacrifice of power conversion efficiencies of the DSSCs. The mild hydrothermal reduction method is believed to be versatile in synthesizing various binary alloy CEs.

2. Experimental

2.1. Preparation of Ru–Se alloy CEs

The feasibility of this strategy was confirmed by following experimental procedures: A mixing aqueous solution consisting of Se powders, $RuCl_3$, and polyvinylpyrrolidone (PVP) was made by agitating Se ultrafine powders (0.001, 0.002, 0.004, 0.006, and 0.01 g), 5 ml of 5 mM $RuCl_3$ aqueous solution, and 1 ml of pure PVP at 60 °C. 2 ml of hydrazine hydrate (85 wt%) was dropped into the above solution, after vigorous agitating for 15 min, the reactant was transferred into a Teflon-lined autoclave and cleaned FTO glass substrate (sheet resistance 12 Ω sq^{-1}, purchased from Hartford Glass Co., USA) with FTO layer downward was immersed in. The total volume of reagent solution was adjusted at 40 ml by adding deionized water. After the reaction at 120 °C for 12 h, the FTO substrate was rinsed by deionized water and vacuum dried at 50 °C.

As references, the Ru-only and Se-only CEs were also prepared according to the above procedures. The Pt CE (300–400 μm in thickness) was purchased from Dalian HepatChroma SolarTech Co., Ltd and used as a standard.

2.2. Assembly of DSSCs

A layer of TiO_2 colloid film with a thickness of 10 μm and area of 0.25 cm^2 was prepared by a sol–hydrothermal method and subsequently calcined at 450 °C for 30 min [25]. The resultant TiO_2 nanocrystalline film was sensitized by immersing into a 0.50 mM ethanol solution of N719 dye (purchased from DYESOL LTD) for 24 h. A DSSC device was fabricated by sandwiching redox electrolyte between a dye-sensitized TiO_2 anode and an FTO supported Ru–Se alloy CE. A redox electrolyte consisted of 100 mM of tetraethylammonium iodide, 100 mM of tetramethylammonium iodide, 100 mM of tetrabutylammonium iodide, 100 mM of NaI, 100 mM of KI, 100 mM of LiI, 50 mM of I_2, and 500 mM of 4-tert-butyl-pyridine in 50 ml acetonitrile.

2.3. Electrochemical characterizations

The electrochemical performances were recorded on a conventional CHI660E setup comprising an Ag/AgCl reference electrode, a CE of platinum sheet, and a working electrode of FTO glass supported RuSe alloy. The cyclic voltammetry (CV) curves were recorded in a supporting electrolyte consisting of 50 mM M LiI, 10 mM I_2, and 500 mM $LiClO_4$ in acetonitrile. Electrochemical impedance spectroscopy (EIS) measurements were carried out in a frequency range of 0.01 Hz–10^6 kHz and at an ac amplitude of 10 mV. Tafel polarization curves were recorded by assembling symmetric cell consisting of binary Ru–Se alloy CE|redox electrolyte|binary Ru–Se alloy CE.

2.4. Photovoltaic measurements

The photocurrent–voltage (J–V) curves of the DSSCs were recorded on an electrochemical workstation (CHI600E) under irradiation of a simulated solar light from a 100 W xenon arc lamp in ambient atmosphere. The incident light intensity was calibrated using a FZ-A type radiometer from Beijing Normal University Photoelectric Instrument Factory to control it at 100 mW cm^{-2} (AM 1.5). Each DSSC device was measured at least five times to eliminate experimental error and a compromise J–V curve was employed.

2.5. Other characterizations

The compositions of the binary Ru–Se alloy CEs were detected by inductively coupled plasma-atomic emission spectra (ICP-AES). Prior to ICP measurements, the CEs were immersed in concentration nitric acid to dissolve the FTO glass substrate thoroughly.

3. Results and discussion

The compositions of the binary Ru–Se alloys on FTO glass substrates are determined by ICP-AES equipment. The results display that the atomic ratios of Ru_2Se, RuSe, $RuSe_2$, $RuSe_3$, and $RuSe_5$ are 1.93: 1.00, 1.00: 0.97, 1.00: 1.88, 1.00: 2.86, and 1.00: 4.82, respectively. The measured atomic ratios are close to the stoichiometry of Ru_2Se, RuSe, $RuSe_2$, $RuSe_3$, and $RuSe_5$, therefore, the chemical formulas of the alloy CEs can be expressed according to their stoichiometric ratios.

To investigate the electrocatalytic activity of the synthesized Ru–Se alloy CEs, cyclic voltammetry (CV) is carried out at a scan rate of 50 mV s^{-1}. Fig. 1 shows the typical voltammograms of various CEs for the redox couples (I^-/I_3^-). Two pairs of redox peaks are observed in Pt CE because of the occurrence of two-step reactions between I_3^- and I^- ions [26]. The CV curves of alloy CEs have similar peak positions and shapes to those of Pt-only CE, indicating that the resultant binary Ru–Se alloy CEs have a similar

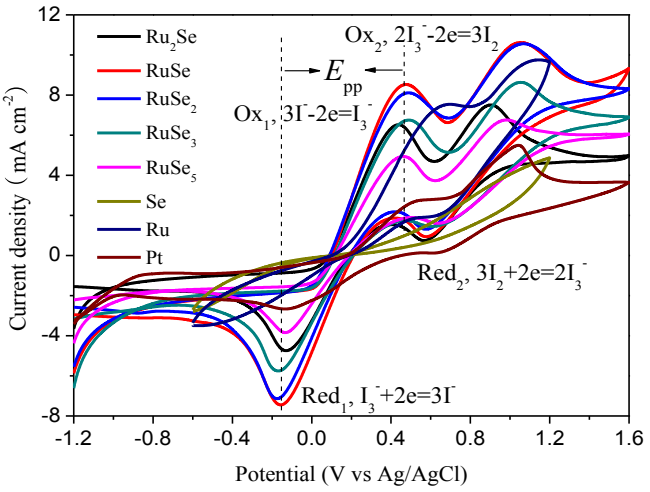

Fig. 1. (a) CV curves of various CEs recorded at a scan rate of 50 mV s^{-1}.

electrocatalytic activity to Pt CE. Considering that the role of a CE is a mediator of reducing I^-/I_3^- redox species in regenerating dye molecules after electron injection in a liquid-state DSSC. Generally, the characteristic Red_1 peak including current density and overpotential can be employed to elevate the electrocatalytic activity of binary Ru–Se alloy CEs [27]. Compared with Pt-only CE, the binary Ru–Se alloy CEs have a similar overpotential and invertibility. The results indicate the smoothness of the redox reaction of I^-/I_3^- on the alloy electrode, which produces favorable conditions for the regeneration of the sensitizer. However, all alloy CEs have higher current densities than Pt's. After a comprehensive analysis for overpotential and current density of the peaks, we make a conclusion that the binary RuSe alloy CE has the highest electrocatalytic activity. However, no obvious redox peaks are observed for pure Ru and Se electrodes, suggesting that Ru and Se electrodes have low electrocatalytic activities toward I_3^- reduction reaction. Considering that the E_{pp} (peak-to-peak separation) is lower than 1000 mV, the reversibility of redox reaction by RuSe CE ($E_{pp} = 623$ mV) is also better than 684 mV for Pt-only CE. The rapid interconversion between I_3^- and I^- ions facilitates the participation in subsequent circles and improves the power conversion efficiency. To elucidate the diffusion of redox ions on alloy CEs, Randles–Sevcik theory is employed and presented [28,29]:

$$J_{red} = Kn^{1.5}ACD_n^{0.5}v^{0.5} \quad (1)$$

where J_{red} is the peak current density of Red_1 (mA cm^{-2}), K is 2.69×10^5, n is the number of electrons of reduction reaction, A is the electrode area (cm^2), C represents the bulk concentration of I_3^- (mol L^{-1}), and D_n is the diffusion coefficient (cm^{-2} s^{-1}). The diffusivity of Pt–only CE is 1.59×10^{-6} cm^{-2} s^{-1} which is comparable to 2.55×10^{-6} cm^{-2} s^{-1} in the literature [30]. The RuSe alloy CE has the highest diffusivity (4.38×10^{-6} cm^{-2} s^{-1}) in comparison with Ru_2Se (2.78×10^{-6} cm^{-2} s^{-1}), $RuSe_2$ (4.17×10^{-6} cm^{-2} s^{-1}), $RuSe_3$ (3.35×10^{-6} cm^{-2} s^{-1}), $RuSe_5$ (2.26×10^{-6} cm^{-2} s^{-1}), Ru (5.78×10^{-7} cm^{-2} s^{-1}), and Pt (9.85×10^{-7} cm^{-2} s^{-1}). The results indicate that the RuSe alloy CE has a similar diffusivity to 4.92×10^{-6} cm^{-2} s^{-1} of poly(3,4–ethylenedioxythiophene) [30]. This is attributed to the large number of highly electrocatalytic RuSe alloy electrode and the abundant active sites, which are able to shorten the ion diffusion path and promote ion diffusion flux [31–33].

From the stacking CV curves of RuSe alloy CE at scan rates from 50 to 200 mV s^{-1}, one can find an outward extension of all the peaks (Fig. 2a). By plotting peak current density corresponding to $I_3^- \leftrightarrow I^-$ versus square root of scan rate, as shown in Fig. 2b, linear relationships are observed. This result indicates the redox reaction on the surface of the binary RuSe alloy CE is controlled by ionic diffusion in the electrolyte, and the transfer rate of both electrons and ions are fast enough for the reduction rate of I_3^- on the surface of RuSe alloy CE. This result also suggests that the adsorption of redox species is hardly affected by the redox reaction on the RuSe alloy CE surface and no specific interaction occurred between I^-/I_3^- couples and the alloy CE.

60 cycles of CV curves in Fig. 3a are used to evaluate stability of RuSe alloy CE and the plots of peak current density as a function of cycle number are given in Fig. 3b. No apparent decline in peak current densities is observed, indicating that the RuSe alloy CE is relatively stable for catalyzing I_3^-.

Electrochemical impedance spectroscopy (EIS) is an effective and widely used tool for investigating the charge transfer process and thereby for evaluating the catalytic activity of an electrocatalyst. Fig. 4 shows the Nyquist plots of the symmetrical dummy cells fabricated with two identical counter electrodes. The intercept on the real axis can be generally attributed to series resistance (R_s). The left arch can be assigned to the charge transfer resistance (R_{ct}), whereas the right arch can be assigned to the Nernst diffusion impedance (W) of the redox couple transport in the electrolyte [34,35]. The EIS data are obtained by fitting the Nyquist plots with an equivalent circuit diagram and summarized in Table 1. The R_s of Pt CE is 20.77 Ω cm^2, whereas it is 3.76, 3.04, 2.49, 3.04, and 3.56 Ω cm^2 for Ru_2Se, RuSe, $RuSe_2$, $RuSe_3$, and $RuSe_5$ alloy CEs, respectively. The lower R_s values in binary Ru–Se alloy CEs indicate a higher electron-conducting ability. Therefore, the RuSe alloy CE has a low electron loss within the alloy layer. The R_{ct} of Pt CE is 7.23 Ω cm^2, while R_{ct} of Ru_2Se, RuSe, $RuSe_2$, $RuSe_3$, and $RuSe_5$ alloy is 6.12, 1.90, 2.87, 3.25, and 26.10 Ω cm^2, respectively. This means

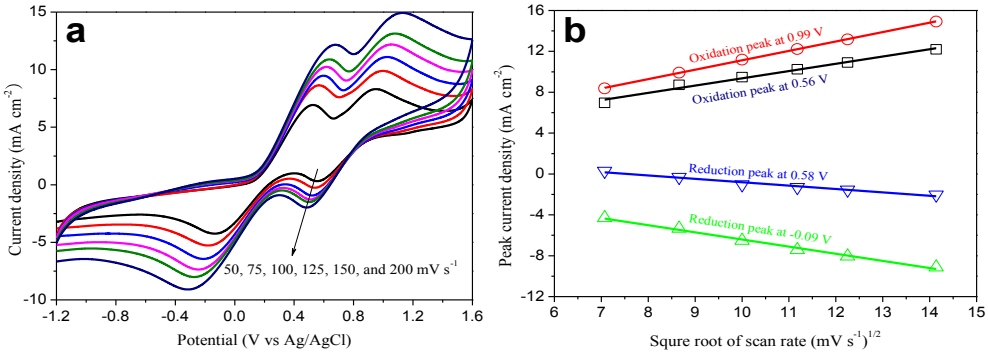

Fig. 2. (a) CV curves of RuSe alloy CE at various scan rates, and (b) relationship between peak current density and square root of scan rate.

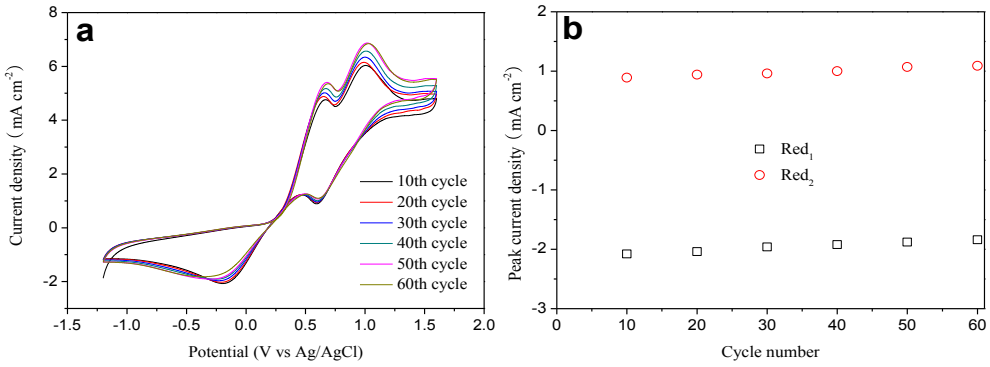

Fig. 3. (a) 60 cycles of CV curves from RuSe alloy CE at a scan rate of 50 mV s^{-1}; (b) relationship between peak current density and cycle number.

that the Ru–Se alloy CEs hold a high electrocatalytic activity for I_3^- reduction. Herein, the RuSe alloy CE shows the highest catalytic activity toward I_3^- ions, which is in an agreement with the results of CV analysis.

Tafel polarization measurements are employed to reconfirm the catalytic activity of the novel Ru–Se alloy electrodes. Fig. 5 displays the Tafel curves of the symmetrical cells which are similar to EIS measurements. The curves show logarithmic current density (log *J*) as a function of potential. Theoretically, the Tafel curve can be divided into three zones. The curve at very high potential is attributed to the limiting diffusion zone, which depends on the transport of I_3^- and I^- in the electrolyte. The curve at relatively low potential but higher than 120 mV corresponds to the Tafel zone, where the voltage is a linear function of log *J*. The curve at very low potential is polarization zone, arising from the electrochemical reaction. In Tafel zone, we can collect information on the exchange current density (J_0, obtained by the intersection of cathodic branch and equilibrium potential line) [24,36–38]. Since J_0 mainly depends on two factors, the concentration of the oxidized species and the electrocatalytic performance of CE. Evidently, the large slope of cathodic and anodic branches is associated with high J_0, which follows an order of RuSe > $RuSe_2$ > $RuSe_3$ > Ru_2Se > $RuSe_5$, which in an agreement with electrocatalysis toward I^-/I_3^- redox couples and charge-transfer ability. The enhanced J_0 demonstrates that alloy CEs can perform as effectively as robust electrocatalysts. The equilibrium potential departed from the location of zero potential, which might be caused by the absorption of I_3^- ions on the CE surface, inducing the interruption in the redox reaction between I_3^- and I^- or by a fast scan rate. Moreover, as a kinetic component arises due to the charge transfer of CE, J_0 is associated with the R_{ct} by the equation [20]:

$$J_0 = RT/nFR_{ct} \quad (2)$$

where *R* is the universal gal constant, *T* is the absolute temperature, *n* is the number of electrons contributing to the charge transfer at the interface, and *F* is Faraday's constant. Therefore, the EIS and Tafel results match well. The good catalytic activity of RuSe alloy CE toward I_3^- ions is expected to elevate the *FF* of DSSCs and therefore the power conversion efficiency. Additionally, limiting diffusion

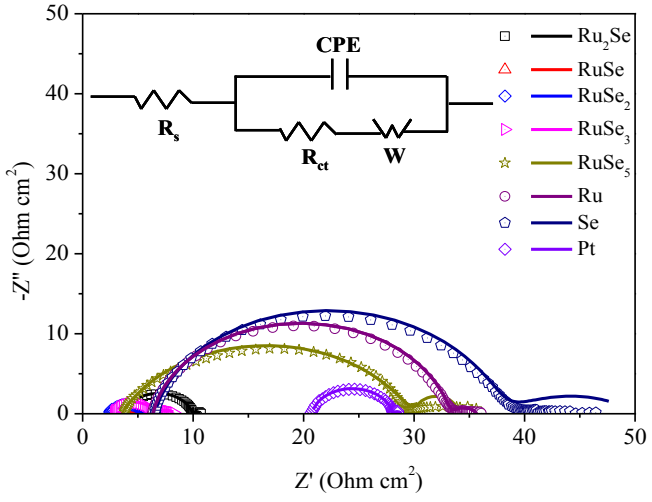

Fig. 4. Nyquist EIS plots for symmetric dummy cells fabricated with two RuSe alloy CEs. The lines express fit results for corresponding EIS data, and the inset gives the equivalent circuit.

Table 1
Parameters for equivalent circuit obtained by fitting EIS data using a Z-view software and from CV curves.

CEs	R_s (Ω cm^2)	R_{ct} (Ω cm^2)	D_n (cm^{-2} s^{-1})
Ru_2Se	3.76	6.12	2.78×10^{-6}
RuSe	3.04	1.90	4.38×10^{-6}
$RuSe_2$	2.49	2.87	4.17×10^{-6}
$RuSe_3$	3.04	3.25	3.35×10^{-6}
$RuSe_5$	3.56	26.10	2.26×10^{-6}
Ru	6.37	26.70	5.78×10^{-7}
Se	6.54	29.96	–
Pt	20.77	7.23	9.85×10^{-7}

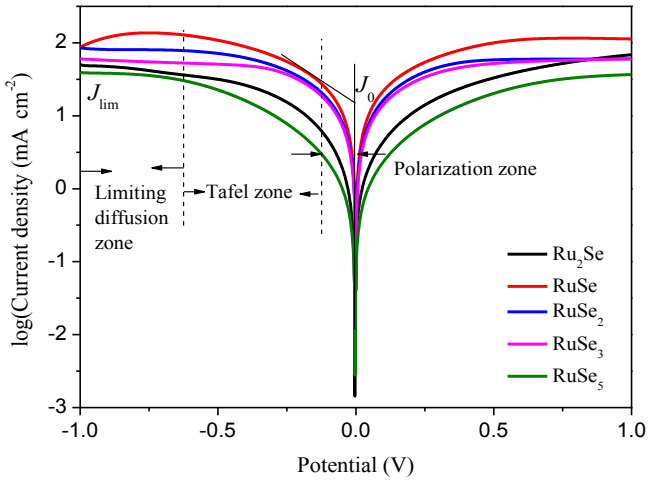

Fig. 5. Tafel polarization curves of symmetrical dummy cells fabricated with two identical RuSe alloy CEs that are the same as the ones used in EIS experiments.

current density (J_{lim}) is determined by the diffusion of the redox species between the two identical CEs, which might have a close relationship with the diffusion impedance from EIS and diffusion coefficient from CV [39]. It can be obtained from the current density at low slope and high potential regions, which depends on the diffusion coefficient of I^-/I_3^- couples in electrolyte. The diffusion coefficient (D_n) of redox couples is in linear with J_{lim} according to Equation (3) [40]:

$$D_n = lJ_{lim}/2nFC \quad (3)$$

where l is the spacer thickness, C is the concentration of I_3^-. J_{lim} values of alloy CEs follow an order of RuSe > $RuSe_2$ > $RuSe_3$ > Ru_2Se > $RuSe_5$, generating an order of D_n: RuSe > $RuSe_2$ > $RuSe_3$ > Ru_2Se > $RuSe_5$. Under the same conditions, a higher D_n suggests an enhanced reaction rate of redox processes during the cell operation. The conclusion is consistent with the result from Equation (1).

Fig. 6a shows the characteristic J–V curves for DSSCs using one of the following catalysts as CEs: RuSe, $RuSe_2$, $RuSe_3$, Ru_2Se, $RuSe_5$, Ru, Se, Pt. The photovoltaic parameters are listed in Table 2. As shown in Fig. 6a, the DSSC using RuSe alloy CE exhibits the highest power conversion efficiency (7.15%) in comparison with 6.62% for $RuSe_2$, 6.36% for $RuSe_3$, 5.84% for Ru_2Se, 4.97% for $RuSe_5$, 5.55% for Ru-only, 3.68% for Se-only, and 5.79% for Pt-only. It is noteworthy to mention that the J_{sc} of 19.05 mA cm^{-2} from RuSe alloy CE based DSSC is much higher than others. This might be attributed to the best electrocatalysis for I_3^- reduction. Moreover, the enhanced charge-transfer ability can also accelerate the recovery of I_3^-. It is noteworthy to mention that RuSe electrode based DSSC has a higher J_{sc} but a lower FF in comparison with Pt electrode. J_{sc} is of dependence on R_{ct}. As shown in Table 1, the R_{ct} of RuSe electrode is 1.90 Ω cm^2 in comparison with 7.23 Ω cm^2 for Pt electrode. However, both R_s and shunt resistance (R_{sh}) have effects on FF. Generally, a lower R_s and higher R_{sh} can result in a higher FF. The R_s of RuSe is lower than that of Pt electrode, but the R_{sh} can not be obtained from the equivalent circuit in symmetric dummy cell. Therefore we can make a deduction that the R_{sh} of RuSe is also lower than that of Pt electrode, leading to a lower FF in its cell device. From the dark J–V curves in Fig. 6b, one can see that the DSSC from RuSe alloy CE shows the smallest dark current density. The dark current in DSSC device is attributed to the I_3^- combination with conduction band electrons of TiO_2 at the TiO_2/electrolyte interface [41]. The smaller dark current indicates that the reduction of I_3^- on the TiO_2/electrolyte interface is retarded and the reduction of I_3^- on the electrolyte/CE interface is relatively efficient [42]. This is another factor for the elevated J_{sc} for RuSe alloy CE based DSSC. After performing a comprehensive analysis of the DSSCs, it can be concluded that the photovoltaic performance is in an agreement with CV, EIS and Tafel polarization results

Table 2
Photovoltaic parameters of the DSSCs. J_{sc}: short-circuit current density; V_{oc}: open-circuit voltage, FF: fill factor; η: power conversion efficiency.

CEs	J_{sc} (mA cm^{-2})	V_{oc} (V)	FF	η (%)
Ru_2Se	12.86	0.675	0.673	5.84
RuSe	19.05	0.673	0.558	7.15
$RuSe_2$	15.39	0.687	0.626	6.62
$RuSe_3$	14.13	0.679	0.663	6.36
$RuSe_5$	13.54	0.681	0.539	4.97
Ru	14.12	0.673	0.584	5.55
Se	10.95	0.643	0.523	3.68
Pt	12.47	0.714	0.650	5.79

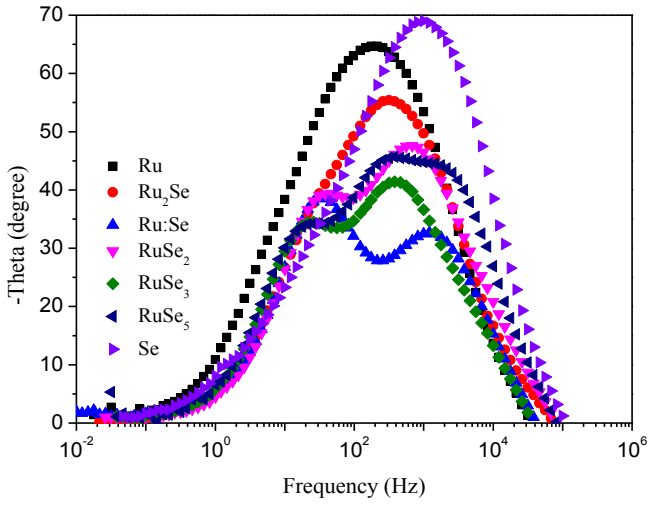

Fig. 7. Bode phase plots of the DSSCs from varied CEs.

To determine the dependence of electron lifetimes of TiO_2 anodes on various CEs, we have recorded the Bode phase plots of assembled DSSC devices (as shown in Fig. 7) and calculated the lifetime using Equation (4) and the related parameters are listed in Table 3.

$$\tau = 1/2\pi f_p \quad (4)$$

where τ is the lifetime of electron on CE, f_p is the peak frequency in Bode EIS plot. The task of a CE is to accelerate the reduction reaction: $I_3^- + 2e \rightarrow 3I^-$, therefore the rapid conversion between I_3^- and

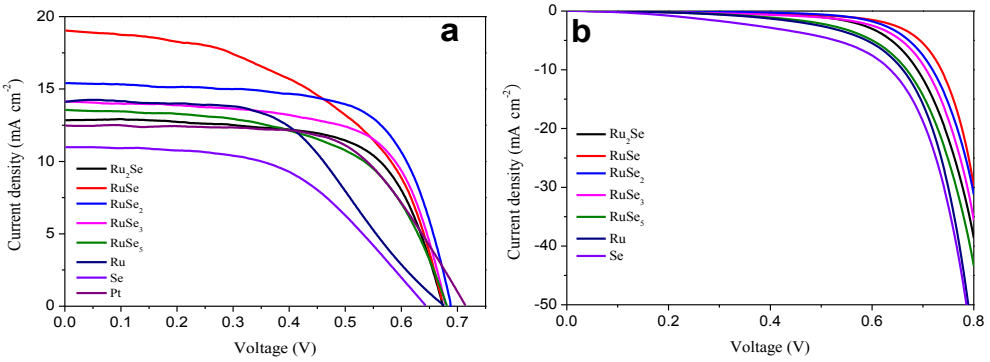

Fig. 6. J–V characteristics of DSSCs from various CEs (a) illuminated under AM 1.5 and (b) in the dark.

Table 3
The peak frequency (f_p) and electron lifetime (τ) of the DSSCs with various CEs.

CEs	f_p (Hz)	τ (ms)
Ru_2Se	323.3	0.49
RuSe	29.3	5.43
$RuSe_2$	36.4	4.37
$RuSe_3$	37.3	4.27
$RuSe_5$	40.5	3.93

I^- species is expected to promote the recovery of organic dyes and therefore electron lifetime in anode. The electrons in TiO_2 anode from RuSe alloy CE based DSSC device have an average lifetime of 5.43 ms, which is higher than 4.37 ms for $RuSe_2$, 4.27 ms for $RuSe_3$, 3.93 ms for $RuSe_5$, 0.49 ms for Ru_2Se. The enhanced electron lifetime in RuSe alloy CE based DSSC can be attributed to the elevated catalytic activity of RuSe alloy CE toward I_3^-. The rapid redox between I_3^- and I^- is expected to accelerate the electron transportation, therefore, the probability of electrons captured by defects is decreased.

4. Conclusions

In summary, we have demonstrated that low-temperature hydrothermal reduction method is an effective strategy in synthesizing RuSe alloy CEs for enhancing the photovoltaic performances of DSSCs. RuSe alloy CE exhibits the best electrocatalytic activity for the reduction of I_3^- ions. The DSSC from RuSe alloy CE provides an impressive power conversion efficiency of 7.15% in comparison with that of 5.79% from Pt-only CE. The research presented here is far from being optimized but these profound advantages along with scalable materials promise the new alloy CEs to be candidates in DSSCs.

Acknowledgments

The authors gratefully acknowledge financial supports from National Natural Science Foundation of China (51102204), Fundamental Research Funds for the Central Universities (201313001, 201312005), Shandong Province Outstanding Youth Scientist Foundation Plan (BS2013CL015), Doctoral Fund of Ministry of Education of China (20130132120023), Shandong Provincial Natural Science Foundation (ZR2011BQ017), and Research Project for the Application Foundation in Qingdao (13-1-4-198-jch).

References

[1] B. O'Regan, M. Grätzel, Nature 353 (1991) 737.
[2] M. Grätzel, Nature 414 (2001) 338.
[3] A. Yella, H.W. Lee, H.N. Tsao, C. Yi, A.K. Chandiran, M.K. Nazeeruddin, E.W. Diau, C.Y. Yeh, S.M. Zakeeruddin, M. Grätzel, Science 334 (2011) 629.
[4] Q.W. Tang, H.Y. Cai, S.S. Yuan, X. Wang, J. Mater. Chem. A 1 (2013) 317.
[5] J.H. Wu, Y. Li, Q.W. Tang, G.T. Yue, J.M. Lin, M.L. Huang, L.J. Meng, Sci. Rep. 4 (2014) 4028.
[6] Q.D. Tai, B. Chen, F. Guo, S. Xu, H. Hu, B. Sebo, X.Z. Zhao, ACS Nano 5 (2011) 3795.
[7] A.J. Nozik, J. Miller, Chem. Rev. 110 (2010) 6443.
[8] Y.M. Xiao, J.Y. Lin, W.Y. Wang, S.Y. Tai, G.T. Yue, J.H. Wu, Electrochim. Acta 90 (2013) 468.
[9] S. Tan, J. Zhai, B. Xue, M. Wan, Q. Meng, Y. Li, L. Jiang, D. Zhu, Langmuir 20 (2004) 2934.
[10] J. Xu, M. Li, L. Wu, Y. Sun, L. Zhu, S. Gu, L. Liu, Z. Bai, D. Fang, W. Xu, J. Power Sources 257 (2014) 230.
[11] G.Q. Wang, W. Xing, S.P. Zhuo, Electrochim. Acta 92 (2013) 269.
[12] J. Han, H. Kim, D.Y. Kim, S.M. Jo, S.Y. Jang, ACS Nano 4 (2010) 3503.
[13] S.H. Seo, M.H. Kim, E.J. Jeong, S.H. Yoon, H.C. Kang, S.I. Cha, D.Y. Lee, J. Mater. Chem. A 2 (2014) 2592.
[14] G.Q. Wang, W. Xing, S.P. Zhuo, Electrochim. Acta 66 (2012) 151.
[15] W. Sun, T. Peng, Y. Liu, S. Xu, J. Yuan, S. Guo, X.Z. Zhao, J. Mater. Chem. A 1 (2013) 2762.
[16] B.L. He, Q.W. Tang, J.H. Luo, Q.H. Li, X.X. Chen, H.Y. Cai, J. Power Sources 256 (2014) 170.
[17] B.L. He, Q.W. Tang, M. Wang, C.Q. Ma, S.S. Yuan, J. Power Sources 256 (2014) 8.
[18] B.L. He, Q.W. Tang, T.L. Liang, Q.H. Li, J. Mater. Chem. A 2 (2014) 3119.
[19] B.L. He, Q.W. Tang, M. Wang, H.Y. Chen, S.S. Yuan, ACS Appl. Mater. Interfaces 6 (2014) 8230.
[20] M.X. Wu, X. Lin, Y. Wang, L. Wang, W. Guo, D. Qi, X. Peng, A. Hagfeldt, M. Grätzel, T.L. Ma, J. Am. Chem. Soc. 134 (2012) 3419.
[21] Q. Xu, F. Liu, Y. Liu, K. Cui, X. Feng, W. Zhang, Y. Huang, Sci. Rep. 3 (2013) 2112.
[22] B.L. He, X. Meng, Q.W. Tang, P.J. Li, S.S. Yuan, P.Z. Yang, J. Power Sources 260 (2014) 180.
[23] B.L. He, X. Meng, Q.W. Tang, ACS Appl. Mater. Interfaces 6 (2014) 4812.
[24] H.Y. Cai, Q.W. Tang, B.L. He, P.J. Li, J. Power Sources 258 (2014) 117.
[25] S.S. Yuan, Q.W. Tang, B.L. He, L. Men, H.Y. Chen, Electrochim. Acta 125 (2014) 646.
[26] N.Q. Fu, Y.Y. Fang, Y.D. Duan, X.W. Zhou, X.R. Xiao, Y. Lin, ACS Nano 6 (2012) 9596.
[27] Q.H. Li, X.X. Chen, Q.W. Tang, H.Y. Cai, Y.C. Qin, B.L. He, M.J. Li, S.Y. Jin, Z.C. Liu, J. Power Sources 248 (2014) 923.
[28] T. Daeneke, A.J. Mozer, T.H. Kwon, N.W. Duffy, A.B. Holmes, U. Bach, L. Spiccia, Energy Environ. Sci. 5 (2012) 7090.
[29] H.Y. Cai, Q.W. Tang, B.L. He, M. Wang, S.S. Yuan, H.Y. Chen, Electrochim. Acta 121 (2014) 136.
[30] Y.M. Xiao, J.Y. Lin, S.Y. Tai, S.W. Chou, G.T. Yue, J.H. Wu, J. Mater. Chem. 22 (2012) 19919.
[31] J.Y. Lin, S.Y. Tai, S.W. Chou, J. Phys. Chem. C 118 (2014) 823.
[32] P. Sudhagar, S. Nagarajan, Y.G. Lee, D. Song, T. Son, W. Cho, M. Heo, K. Lee, J. Won, Y.S. Kang, ACS Appl. Mater. Interfaces 3 (2011) 1838.
[33] Y. Tang, X. Pan, C. Zhang, S. Dai, F. Kong, L. Hu, Y. Sui, J. Phys. Chem. C 114 (2010) 4160.
[34] B. Lei, G.R. Li, X.P. Gao, J. Mater. Chem. A 2 (2014) 3919.
[35] H.M. Chuang, C.T. Li, M.H. Yeh, C.P. Lee, R. Vittal, K.C. Ho, J. Mater. Chem. A 2 (2014) 5816.
[36] M. Tathavadekar, M. Biswal, S. Agarkar, L. Giribabu, S. Ogale, Electrochim. Acta 123 (2014) 248.
[37] Q.H. Li, X.X. Chen, Q.W. Tang, H.T. Xu, B.L. He, Y.C. Qin, J. Mater. Chem. A 1 (2013) 8055.
[38] X.L. Duan, Z. Gao, J. Chang, D. Wu, P. Ma, J. He, F. Xu, S. Gao, K. Jiang, Electrochim. Acta 114 (2013) 173.
[39] M. Al-Mamun, J.Y. Kim, K.J. Lee, Y.H. Ko, J.H. Lee, I.S. In, J.W. Lee, Y.E. Sung, S.R. Kim, Synth. Met. 177 (2013) 77.
[40] M.K. Wang, A.M. Anghel, B. Marsan, N.L.C. Ha, N. Pootrakulchote, S.M. Zakeeruddin, M. Grätzel, J. Am. Chem. Soc. 131 (2009) 15976.
[41] Z.Y. Tang, J.H. Wu, M. Zheng, J.H. Huo, Z. Lan, Nano Energy 2 (2013) 622.
[42] R. Gao, L. Wang, B. Ma, C. Zhan, Y. Qiu, Langmuir 26 (2010) 2460.